# Dalton Transactions



# COMMUNICATION

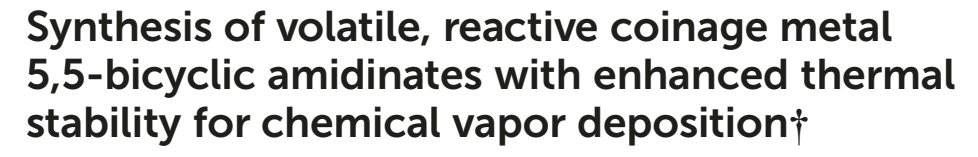
View Article Online



Cite this: DOI: 10.1039/c9dt01202h

Received 20th March 2019, Accepted 29th April 2019 DOI: 10.1039/c9dt01202h

rsc.li/dalton



Liuchuan Tong,  $\bigcirc$  a Luke M. Davis,  $\bigcirc$  ‡ Xian Gong,  $\bigcirc$  b Jun Feng,  $\bigcirc$  § Eugene S. Beh  $\bigcirc$  ¶ and Roy G. Gordon  $\bigcirc$  \* A.b.

Many microelectronic devices require thin films of silver or gold as wiring layers. We report silver(i) and gold(i) bicyclic amidinate complexes, wherein the constrained ligand geometry lessens the propensity for thermal decomposition. These new volatile compounds provide metallic films of silver and gold during CVD with hydrogen below 230 °C.

As microelectronic device features shrink and new, three-dimensional architectures are adopted, the demand grows for new methods to coat and fill these narrow or enclosed features. Chemical vapor deposition (CVD) and atomic layer deposition (ALD) are routinely used in the semiconductor industry for depositing conformal thin films in features with high aspect ratios. The key to the success of new CVD and ALD processes is the development of volatile, thermally stable, yet highly reactive metal precursors. Gold and silver are particularly important contact metals in a variety of circuits.

Even though copper can be deposited from a number of CVD precursors, 7-14 relatively few gold and silver CVD precursors are known. 15-20 Whereas alkyl-substituted amidinate ligands stabilize and volatilize many metal CVD and ALD precursors, 10,11,21-23 silver and gold amidinates with alkyl substituents can be difficult to prepare and tend to decompose during sublimation or upon exposure to light, 11,24,25 which can limit their application in vapor deposition. Several aryl-

One common explanation for thermal instability in coinage metal alkylamidinates is the migration of a  $\beta$ -hydrogen to the metal, cleaving the metal–nitrogen bond and forming an unstable metal hydride. Amidinates lacking  $\beta$ -hydrogens and having cyclic backbones have been employed to suppress this decomposition pathway. Barry and coworkers prepared silver(i) and gold(i) *tert*-butylimino-2,2-dimethylpyrrolidinates, combining these strategies and improving thermal stability to 170 °C. Silver and gold films can be grown with these single-source CVD precursors *via* thermolysis; however, the gold films are carbon-contaminated and poorly conductive ( $\rho$  = 5580  $\mu\Omega$  cm, *cf.* 2.44  $\mu\Omega$  cm for bulk gold). The *tert*-butyl group in the ligand may undergo  $\beta$ -methyl migration to gold, providing an easily accessed carbon source.

We have recently reported the synthesis of the purpose-designed, fully  $\beta$ -substituted 5,5-bicyclic amidine ligand 1, and its copper(i) complex (Scheme 1).<sup>32</sup> The lack of  $\beta$ -hydrogens prevents  $\beta$ -hydride elimination, and the bicyclic system constrains bond rotations to make  $\beta$ -methyl migration reactions unlikely.<sup>32</sup> Consistent with this goal, the solution thermal decomposition rate of 2,<sup>32</sup> a dimeric copper(i) complex of 1, is  $10\times$  slower than that of a previously reported<sup>11</sup> acyclic copper(i) amidinate. Encouraged by this result, we investigated the ability of bicyclic 1 to form volatile gold and silver CVD compounds. Herein we report the synthesis of volatile gold(i) and silver(i) complexes of 1, and demonstrate their use in CVD of gold and silver thin films.

The synthesis of the gold(i) complex 3 is analogous to the synthesis of the copper(i) complex 2 (Scheme 1). Although AuCl can be used to prepare 3, its more soluble dimethylsulfide adduct,  $AuCl(SMe_2)$ , approvides improved yields. Treatment of a THF solution of 1 with KHMDS, followed by transmetalation with  $AuCl(SMe_2)$ , affords the gold(i) amidinate complex 3. During the reaction, the suspension turns purple, indicating the formation of  $Au^0$  nanoparticles as a side

substituted amidinates of silver(I) and gold(I) are known, <sup>26–30</sup> but compounds with aryl substituents rarely have high volatility.

<sup>&</sup>lt;sup>a</sup>Department of Chemistry and Chemical Biology, Harvard University, Cambridge, MA 02138, USA. E-mail: gordon@chemistry.harvard.edu

<sup>&</sup>lt;sup>b</sup>Harvard John A. Paulson School of Engineering and Applied Sciences, Harvard University, Cambridge, MA 02138, USA

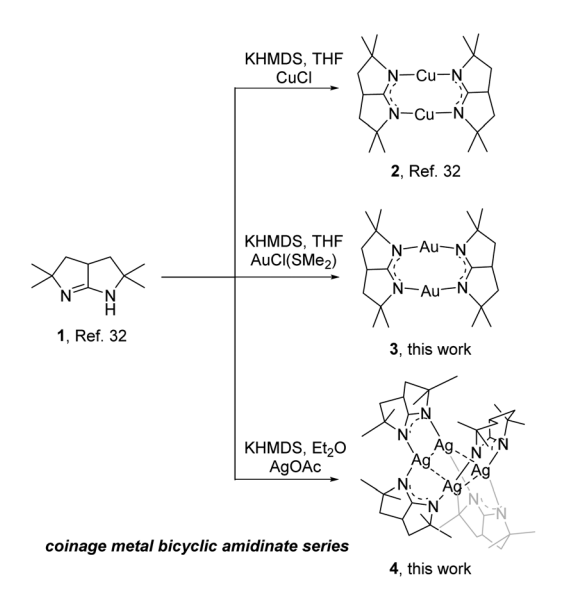
<sup>†</sup>Electronic supplementary information (ESI) available: Full experimental details and spectra. CCDC 1888869 and 1888870. For ESI and crystallographic data in CIF or other electronic format see DOI: 10.1039/c9dt01202h

<sup>‡</sup>Present address: Department of Chemistry, Tufts University, 62 Talbot Avenue, Medford, MA 02155, USA.

<sup>§</sup> Present address: Applied Materials Inc., 1140 E Arques Ave, Sunnyvale, CA 94085. USA.

<sup>¶</sup>Present address: Palo Alto Research Center, 3333 Coyote Hill Road, Palo Alto, CA 94304, USA.

Communication **Dalton Transactions** 



Scheme 1 Synthetic routes to complexes 2, 3, and 4.

product. Filtration of the purple suspension gives a clear solution, which affords white 3 in 60% yield upon concentration, and 3 may be further purified by recrystallization from CH<sub>2</sub>Cl<sub>2</sub> or by sublimation at 170 °C and 30 mTorr. Compound 3 is poorly soluble in THF, requiring large amounts of THF to ensure all product dissolves during filtration. Importantly, 3 does not decompose for several weeks in air, and therefore the purification steps can be carried out in air without loss of yield.

The <sup>1</sup>H NMR spectrum of 3 is similar to that of 2 (Fig. S1-3†). As in 2, splitting of the methyl group signals appears to indicate the presence of two diastereomers.

Single-crystal X-ray diffraction confirmed that the gold(1) complex 3 possesses the same solid-state dimeric structure as the copper(1) complex 2 (Fig. 1a and Tables S1, 2, 4, 6†). Gold(1) amidinates and guanidinates typically adopt dimeric<sup>24,30,34</sup> or tetrameric structures, 35-38 depending on the steric demand of

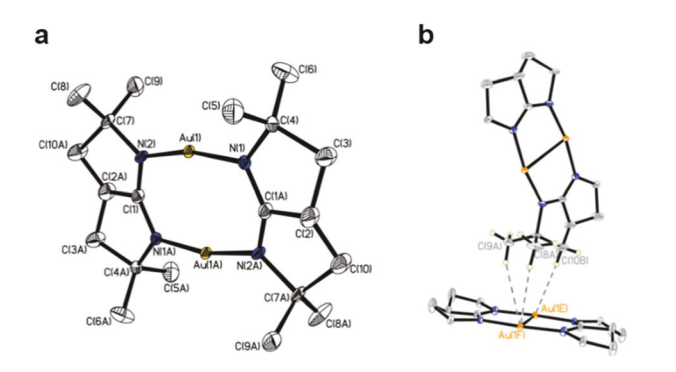


Fig. 1 (a) Solid-state structure of 3 with 50% probability thermal ellipsoids; hydrogen atoms are omitted for clarity. Selected distances (Å) and angles (°): Au-N 2.013(3), Au(1)····Au(1A) 2.855(1); N(1)-Au(1)-N(2) 167.4(1). (b) Gold(i)-methyl interactions between two neighboring molecules. Metrics are given in Table S6.†

the ligand. One of these tetramers is a gold(1) complex of 1,4,6triazabicyclo[3.3.0]oct-4-ene,35 the non-methylated guanidine analogue of 1, suggesting that in 3 the four methyl groups per ligand may contribute to the preference for a dimeric structure.

The gold atoms and the amidinate N-C-N cores form a single plane, with symmetric Au-N distances of 2.013(3) Å that fall on the short end of typical gold(I) amidinates. 24,30,34-39 The Au...Au distance of 2.855(1) Å is long for a digold(1) amidinate, in which this distance is typically 2.644(2)-2.711(3)  $\rm{\mathring{A}}.^{24,30,34,39}$ The ring-constrained N-C-N angle is also larger than usual, at 131.9(2)° (cf. 121.8(5)–128.6(5)° in gold(I) amidinates). 24,30,34–39

Interestingly, molecules of 3 pack face-to-edge (Fig. 1b, S7 and Table S6†), with three neighboring methyl groups pointing at each planar face of the molecule. A recent review of Au···H-C interactions describes as hydrogen bonding AuI...H-C distances Au<sup>I</sup>···H <3 Å and Au<sup>I</sup>···C <4 Å, preferably with the Au<sup>I</sup>···H-C angle approaching 180°. 40 Two of the three methyl groups meet this definition, and the third is just 0.2 Å longer. Thus, each molecule has two or three weak gold(I)-methyl contacts on each face, which may stabilize the solid-state packing of 3.

Synthesis of the silver(1) analogue 4 presented more challenges than the gold and copper counterparts. Despite previous efforts often employing AgCl to synthesize silver amidinate compounds, 11,25 the reaction of AgCl with the deprotonated form of 1 was incomplete after several days of stirring, likely owing to the low solubility of AgCl.

After some screening, AgOAc was selected as the silver(1) source since it has higher solubility in organic solvents. Treatment of a solution of 1 in diethyl ether with KHMDS, followed by transmetalation with AgOAc, gave the silver(1) complex 4. Filtration of the brown suspension, presumably colored by some Ago nanoparticles, gave a clear brown solution. Compound 4 was obtained as white solids in 45% yield upon concentration of this liquor. Similar to 3, the silver(1) amidinate 4 is stable in air for several weeks.

The <sup>1</sup>H NMR spectrum of 4 contains many more peaks than the spectrum of 2 or 3 (Fig. S4-5†). Microanalysis indicated the correct stoichiometry, though, and the product NMR spectrum remained unchanged after sublimation at 160 °C and 30 mTorr. Consistent with these data, single-crystal X-ray diffraction revealed compound 4 to be the authentic silver(1) complex, but having a tetrameric structure (Fig. 2a and Tables S1, 3, 5†) instead of sharing the dimeric structures of 2 and 3. Although silver(I) amidinates are usually dimers 11,26,27,34,41 or trimers, 11,24 tetrameric amidinates 28 and a guanidinate 42 are

The tetranuclear silver(1) core of 4 forms a rhombus, with sides 3.296(2) Å and diagonal 3.096(2) Å (Ag(1)···Ag(1A)); these side distances are longer than the distances of 2.807(1)-2.920(1) Å found in related tetramers. 28,42 The ligands bridge between silver atoms, in an alternating up-down-up-down fashion around the ring. As in 3, the Ag-N distances in 4, 2.054(2) and 2.094(2) Å, are among the shorter distances found 2.076(4) - 2.140(4)tetrasilver(1) amidinates,

**Dalton Transactions** 

Fig. 2 (a) Solid-state structure of 4 with 50% probability thermal ellipsoids. Hydrogen atoms and minor disorder component (25%) are omitted for clarity. Selected distances (Å) and angles (°): Ag(1)-N(1) 2.094(2), Ag(2)-N(2) 2.054(2); N(1)-Ag(1)-N(1A) 165.5(1), N(2)-Ag(2)-N(2A) 178.0(1). (b) View of the asymmetric unit, with both disorder components shown; closed (black) bonds indicate the major component (75%), and open (white) bonds indicate the minor component (25%). The 35% thermal ellipsoids are shown, with hydrogen atoms omitted for clarity.

Constrained by its 5,5-bicycle, the amidinate N-C-N angle is unusually large: 131.9(2)°, vs. typical values of 119.0(7)°-125.6(2) . 11,24,34,42

The best structural model of 4 has a disorder component that refines to represent 25% of the ligands (Fig. 2b). This 25% has the conformation with the methine hydrogen pointing away from the Ag4 core. The combination of the tetrameric structure and multiple stereoisomers presumably gives rise to the more complicated NMR spectrum of 4.

Thermogravimetric analysis (TGA) was performed in a nitrogen-filled glovebox to study the thermal stability and evaporation rate of 2-4 (Fig. 3). As reported previously, 32 2 sublimes cleanly under a linear temperature ramp, with 50% mass loss at 270 °C and <0.2 wt% of residue. In contrast, the gold(I) compound 3 had two weight loss regions overlapping each other, with the second starting at around 310 °C. After heating to 500 °C, ~25 wt% remained, along with a purple residue on the TGA pan. Presumably this material is gold nanoparticles generated by thermolysis of 3, which begins at a higher temperature than the sublimation onset. More surprising was the TGA of silver(1) compound 4. Although the silver compound exists

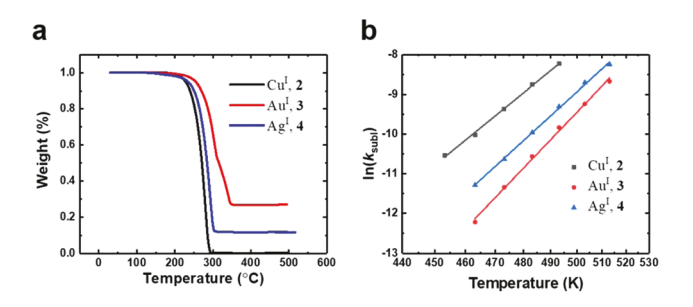


Fig. 3 (a) Ramp TGA of compounds 2, 3, and 4. A linear ramp of 10 °C min<sup>-1</sup> was used, with a sample mass of ca. 10 mg. (b) Arrhenius plot of stepped-isothermal TGA. Each temperature was held for 11 min. The temperature is plotted in reciprocal scale. Data for 2 adapted from ref. 32.

as a tetramer in the solid state, 4 had a mass loss profile similar to that of 2, except with ca. 12 wt% residue. It is hypothesized that the tetrameric silver(1) compound may rearrange to a dimer upon heating, resulting in evaporation kinetics in line with dimeric 2 and 3 (Fig. S6†).

CVD precursors should sublime without decomposition in the CVD sublimation chamber. Clear evidence of degradation in the ramp TGA curves made it difficult to judge whether there would be sublimation-only regions for 3 and 4. Therefore, we conducted isothermal TGA experiments at temperatures between 180 and 240 °C. The resulting evaporation rates were plotted on a log-reciprocal plot, Fig. 3b; linearity on this plot confirms a single mass-loss mechanism in the studied temperature range. Making the usual assumption about constant surface area, effective enthalpies of sublimation can be extracted from these plots. Compound 2 has an enthalpy of sublimation of 109 kJ mol<sup>-1</sup>, as reported earlier;<sup>32</sup> complexes 3 and 4 have sublimation enthalpies of 140 and 122 kJ mol<sup>-1</sup>, respectively. Especially given that metal-nitrogen bond lengths are typically shorter in gold(I) than in silver(I) complexes of the same amidinate ligand, 11,24,26,30,34,35,39,42 and therefore the gold molecules are smaller, it is tempting to propose that the gold(1)-methyl interactions described above contribute to the higher sublimation enthalpy of 3 compared with 4.

With new, sublimable silver(1) and gold(1) compounds in hand, we sought to evaluate their suitability as CVD precursors. Silver and gold metal films were deposited in a custombuilt CVD system (Scheme S1†), using precursor vapor carried by nitrogen or argon and molecular hydrogen as the reductant. During the deposition process, the vaporized precursor was carried with a constant flow of 100 sccm of inert gas, and then mixed with purified hydrogen gas before reaching the preheated reaction chamber. The temperature of the precursor was maintained at various values from 160 to 180 °C for both silver and gold depositions. Substrate temperatures of 200-230 °C were explored for both silver and gold depositions.

Fig. 4a and b shows the cross-sectional and plan-view scanning electron micrographs of gold and silver films deposited from 3 and 4 in the presence of H2. Small crystalline grains were observed in both gold and silver films. Film thickness was measured in the cross-sectional images, and the effective growth rate extracted using the CVD reaction time (Tables S7 and 8†).

Film composition and purity were determined using X-ray photoelectron spectroscopy (XPS). Survey scans of gold and silver films are shown in Fig. 4c and d; gold and silver are the primary components. Fine scans of the C 1s region (Fig. S8†), reveal 5.9 at% and 6.6 at% of carbon in gold and silver films, respectively. No oxygen peaks can be detected in XPS fine scans. Our conditions deposit gold and silver films of good purity.

Gold and silver films both displayed a mirror-like finish (Fig. S9a†). A positive linear relation was observed between the precursor reservoir temperature and the CVD growth rate for both metals (Fig. S9b†), presumably resulting from higher

Communication

Fig. 4 Film characterization; SEM images of (a) a gold film, and (b) a silver film. XPS survey scans of the optimal film at the deepest etching level for (c) gold and (d) silver.

Binding Energy (eV)

Binding Energy (eV)

evaporation rates providing greater precursor flux. The data show a higher growth rate for silver than for gold at a given reservoir temperature, consistent with the higher enthalpy of sublimation of 3. Given the low, flux-limited growth rates (<0.26 nm min<sup>-1</sup>), the growth may depend on reactor geometry, and these precursors might benefit from direct liquid evaporation. Alternatively, ligand modifications to reduce solid-state intermolecular interactions might be beneficial.

No gold film was obtained without hydrogen gas as a coreactant, confirming that the pure gold films were produced by hydrogen reduction of 3 instead of thermal decomposition. For the silver precursor 4, films were obtained even in the absence of molecular hydrogen due to parasitic thermal decomposition of the silver precursor at 230 °C. However, this silver film was ~40 at% carbon by XPS and was not electrically conductive.

Electrical resistivity was measured for both gold and silver films using a four-point probe and a Hall effect measurement system. In the case of gold films, a variety of deposition conditions provided low resistivities, in the range of 22.2–25.1  $\mu\Omega$  cm (Table S7†); these values are within one order magnitude of bulk gold (2.44  $\mu\Omega$  cm). The resistivity of silver films ranged from 19.2  $\mu\Omega$  cm to 220  $\mu\Omega$  cm (Table S8†). The purest silver film has the lowest resistivity, 19.2  $\mu\Omega$  cm, also near an order of magnitude over bulk silver (1.59  $\mu\Omega$  cm); different carbon impurity levels may drive resistivity differences between CVD conditions.

In summary, volatile homoleptic gold(1) and silver(1) amidinates were synthesized by reactions of metal(1) sources with alkali metal amidinates. The tetrameric silver complex 4 is believed to rearrange into a dimer similar to the gold complex 3 upon heating. Both 3 and 4 show remarkable stability to air, light, and heat while retaining reactivity with molecular hydrogen. Metallic gold and silver films were obtained by CVD with hydrogen. Films with good purity and conductivity could be

obtained at substrate temperatures below 230 °C. Our work illustrates the power of bicyclic amidinate ligands to support reactive and volatile transition metal compounds with enhanced thermal stability relative to previous state-of-the-art ligands, opening up the possibility of further advances in the vapor deposition of challenging-to-deposit metals.

## Conflicts of interest

Harvard University has filed a patent application based on the compounds described here.

# Acknowledgements

This research was supported by the US National Science Foundation #1764338, Department of Energy #DE-AC36-08GO28308, Office of Naval Research #N00014-10-0937, Defense Advanced Research Projects Agency #SC001-0000000950 and #FA8650-15-C-7543, and TEL Technology Center, America LLC #A33073. Some of the work was performed at Harvard University's Center for Nanoscale Systems (CNS), a member of the National Nanotechnology Infra-Structure Network (NNIN).

# Notes and references

- 1 A. C. Jones and M. L. Hitchman, *Chemical Vapour Deposition: Precursors, Processes and Applications*, RSC Publishing, Cambridge, 2009.
- 2 S. M. George, Chem. Rev., 2010, 110, 111.
- 3 R. G. Gordon, in *Atomic Layer Deposition for Semiconductors*, ed. C. S. Hwang and C. Y. Yoo, Springer US, New York, 2014, p. 15.
- 4 R. W. Johnson, A. Hultqvist and S. F. Bent, *Mater. Today*, 2014, 17, 236.
- 5 M. Putkonen and L. Niinistö, in *Precursor Chemistry of Advanced Materials*, ed. R. A. Fischer, Springer Berlin Heidelberg, Berlin, Heidelberg, 2005, p. 125.
- 6 J. Hämäläinen, M. Ritala and M. Leskelä, *Chem. Mater.*, 2014, **26**, 786.
- 7 T. J. Wenzel, E. J. Williams, R. C. Haltiwanger and R. E. Sievers, *Polyhedron*, 1985, 4, 369.
- 8 P. Maårtensson and J. O. Carlsson, *J. Electrochem. Soc.*, 1998, **145**, 2926.
- 9 K.-H. Park and W. J. Marshall, *J. Am. Chem. Soc.*, 2005, **127**, 9330.
- 10 Z. Li, S. T. Barry and R. G. Gordon, *Inorg. Chem.*, 2005, 44, 1728.
- 11 B. S. Lim, A. Rahtu, J.-S. Park and R. G. Gordon, *Inorg. Chem.*, 2003, 42, 7951.
- 12 J. P. Coyle, W. H. Monillas, G. P. A. Yap and S. T. Barry, *Inorg. Chem.*, 2008, 47, 683.

Dalton Transactions Communication

- 13 J. W. Park, H. S. Jang, M. Kim, K. Sung, S. S. Lee, T.-M. Chung, S. Koo, C. G. Kim and Y. Kim, *Inorg. Chem. Commun.*, 2004, 7, 463.
- 14 V. V. Grushin and W. J. Marshall, Adv. Synth. Catal., 2004, 346, 1457.
- 15 Z. Yuan, N. H. Dryden, J. J. Vittal and R. J. Puddephatt, *Chem. Mater.*, 1995, 7, 1696.
- 16 Z. Yuan, N. H. Dryden, X. Li, J. J. Vittal and R. J. Puddephatt, J. Mater. Chem., 1995, 5, 303.
- 17 K.-M. Chi and Y.-H. Lu, Chem. Vap. Deposition, 2001, 7, 117.
- 18 L. Gao, P. Härter, C. Linsmeier, A. Wiltner, R. Emling and D. Schmitt-Landsiedel, *Microelectron. Eng.*, 2005, 82, 296.
- 19 E. Szłyk, P. Piszczek, I. Łakomska, A. Grodzicki, J. Szatkowski and T. Błaszczyk, *Chem. Vap. Deposition*, 2000, **6**, 105.
- 20 R. G. Parkhomenko, A. E. Turgambaeva, N. B. Morozova, S. V. Trubin, V. V. Krisyuk and I. K. Igumenov, *Chem. Vap. Deposition*, 2013, 19, 38.
- 21 B. S. Lim, A. Rahtu and R. G. Gordon, *Nat. Mater.*, 2003, 2, 749.
- 22 O. M. El-Kadri, M. J. Heeg and C. H. Winter, *Dalton Trans.*, 2006, 4506.
- 23 Z. Li, R. G. Gordon, V. Pallem, H. Li and D. V. Shenai, Chem. Mater., 2010, 22, 3060.
- 24 T. J. J. Whitehorne, J. P. Coyle, A. Mahmood, W. H. Monillas, G. P. A. Yap and S. T. Barry, Eur. J. Inorg. Chem., 2011, 3240.
- 25 J. P. Coyle, P. G. Gordon, A. P. Wells, D. J. Mandia, E. R. Sirianni, G. P. A. Yap and S. T. Barry, *Chem. Mater.*, 2013, 25, 4566.
- 26 A. C. Lane, M. V. Vollmer, C. H. Laber, D. Y. Melgarejo, G. M. Chiarella, J. John, P. Fackler, X. Yang, G. A. Baker and J. R. Walensky, *Inorg. Chem.*, 2014, 53, 11357.
- 27 S. J. Archibald, N. W. Alcock, D. H. Busch and D. R. Whitcomb, *Inorg. Chem.*, 1999, 38, 5571.

- 28 S. J. Archibald, N. W. Alcock, D. H. Busch and D. R. Whitcomb, *J. Cluster Sci.*, 2000, **11**, 261.
- 29 F. A. Cotton, X. Feng, M. Matusz and R. Poli, J. Am. Chem. Soc., 1988, 110, 7077.
- 30 H. E. Abdou, A. A. Mohamed, J. John and P. Fackler, *Inorg. Chem.*, 2005, **44**, 166.
- 31 J. P. Coyle, A. Kurek, P. J. Pallister, E. R. Sirianni, G. P. A. Yap and S. T. Barry, *Chem. Commun.*, 2012, 48, 10440.
- 32 E. S. Beh, L. Tong and R. G. Gordon, *Organometallics*, 2017, 36, 1453.
- 33 M.-C. Brandys, M. C. Jennings and R. J. Puddephatt, J. Chem. Soc., Dalton Trans., 2000, 4601.
- 34 D. Fenske, G. Baum, A. Zinn and K. Dehnicke, *Z. Naturforsch.*, *B: J. Chem. Sci.*, 1990, 45, 1273.
- 35 A. A. Mohamed, A. P. Mayer, H. E. Abdou, M. D. Irwin, L. M. Pérez, J. John and P. Fackler, *Inorg. Chem.*, 2007, 46, 11165.
- 36 H. E. Abdou, A. A. Mohamed, J. M. López-de-Luzuriaga, J. John and P. Fackler, J. Cluster Sci., 2004, 15, 397.
- 37 A. A. Mohamed, H. E. Abdou, M. D. Irwin, J. M. López-de-Luzuriaga, J. John and P. Fackler, J. Cluster Sci., 2003, 14, 253.
- 38 E. Hartmann and J. Strähle, Z. Naturforsch., B: J. Chem. Sci., 1989, 44, 1.
- 39 S. K. Adas, J. A. Ocana and S. D. Bunge, *Aust. J. Chem.*, 2014, 67, 1021.
- 40 H. Schmidbaur, H. G. Raubenheimer and L. Dobrzanska, *Chem. Soc. Rev.*, 2014, 43, 345.
- 41 S. Wang, N. Harmgarth, P. Leibing and F. T. Edelmann, *Acta Crystallogr., Sect. E: Crystallogr. Commun.*, 2016, 72, 1786.
- 42 M. D. Irwin, H. E. Abdou, A. A. Mohamed, J. John and P. Fackler, *Chem. Commun.*, 2003, 2882.

Synthesis of Volatile, Reactive Coinage Metal 5,5-Bicyclic Amidinates with Enhanced Thermal Stability for Chemical Vapor Deposition

Liuchuan Tong, Luke M. Davis, Xian Gong, Jun Feng, Eugene S. Beh, and Roy G. Gordon

Department of Chemistry and Chemical Biology, Harvard University, Cambridge, MA 02138 Email: gordon@chemistry.harvard.edu

# **SUPPORTING INFORMATION**

**General information:** <sup>1</sup>H NMR and <sup>13</sup>C NMR spectra were recorded on Varian Unity INOVA 500 spectrometers at 11.7 T in the Laukien-Purcell Instrumentation Center Magnetic Resonance Lab at Harvard University. NMR spectra were recorded in solutions of deuterated chloroform (CDCl<sub>3</sub>) with the residual chloroform (7.24 ppm for <sup>1</sup>H NMR and 77.23 ppm for <sup>13</sup>C NMR) taken as the internal standard, or deuterated benzene (C<sub>6</sub>D<sub>6</sub>) with residual benzene (7.16 ppm for <sup>1</sup>H NMR and 128.39 ppm for <sup>13</sup>C NMR) taken as the internal standard, and were reported in parts per million (ppm). Mass spectra were recorded at the Harvard University mass spectrometry facility on a Bruker microTOF-QII instrument using a direct injection method with 0.1% formic acid, 50% water in acetonitrile as the mobile phase. Elemental analyses were performed by the University of Illinois at Urbana-Champaign Microanalysis lab. X-ray crystallographic data were collected at the Harvard University X-Ray Facility on a Bruker APEX DUO single crystal diffractometer. All reactions sensitive to moisture or oxygen were carried out in oven dried or flame dried and nitrogen-charged glassware, or in an argon-filled glovebox. Anhydrous solvents were saturated with nitrogen and dried with 4A molecular sieves purchased from Sigma-Aldrich. All other solvents and reagents were used as received from commercial suppliers without prior purification unless otherwise specified. The purity and identity of all new organic compounds was determined by NMR and mass spectrometry. The metal-containing compounds reported in this paper were also characterized by elemental analysis.

The compounds 3-(2-amino-2-methylpropyl)-5,5-dimethylpyrrolidin-2-one and copper(I) 2,2,5,5-tetramethyl-1,2,3,3a,4,5-hexahydropyrrolo[2,3-b]pyrrolide (compound **2**) were prepared by the previously reported methods.<sup>1</sup> 2,2,5,5-tetramethyl-1,2,3,3a,4,5-hexahydropyrrolo[2,3-b]pyrrole, **1**, was prepared by modification of the literature route, <sup>1</sup> as described below.

#### Synthesis and characterization

1

2,2,5,5-tetramethyl-1,2,3,3a,4,5-hexahydropyrrolo[2,3-b]pyrrole, compound 1. 3-(2-amino-2methylpropyl)-5,5-dimethylpyrrolidin-2-one<sup>1</sup> (15 g, 81.4 mmol) was dissolved in 200 mL of acetonitrile. To the solution was added N,O-bis(trimethylsilyl)acetamide (BSA, 33.5 g, 160.0 mmol) over 3 hours. The solution was refluxed for 2 days, during which the progress of the reaction was monitored by NMR and more BSA was added if the NMR spectra indicated incomplete reaction (Scheme  $S\alpha$ ). Once the reaction was complete, the solution was concentrated in vacuo and the resulting oil was dissolved in 200 mL of 3.0 M HCl and washed with CH<sub>2</sub>Cl<sub>2</sub> (3 × 100 mL), then ice was added and 1 was precipitated by slowly adding 125 mL of cold 5.0 M NaOH. The suspension was then extracted with CH<sub>2</sub>Cl<sub>2</sub> (4 × 100 mL), and the extracts were combined, dried over anhydrous sodium sulfate, and evaporated to afford crude 1 as a pale-yellow waxy solid. Oily impurities were collected by sublimation at 45 °C at 50 mTorr for 2 hours and discarded. Further sublimation of the remaining solid overnight at 70 °C at 50 mTorr gave pure, anhydrous 1 (7.4 g, 55%) as a white solid suitable for the synthesis of metal-containing CVD precursors, mp. 182-183 °C. <sup>1</sup>H NMR (500 MHz, C<sub>6</sub>D<sub>6</sub>) δ 9.20-8.45 (bs, 1H), 3.22-3.14 (m, 1H), 1.73-1.66 (m, 2H), 1.33 (s, 6H), 1.29-1.23 (m, 2H), 1.17 (s, 6H);  ${}^{13}$ C NMR (125 MHz, C<sub>6</sub>D<sub>6</sub>)  $\delta$ 174.9, 69.8, 46.2, 45.3, 31.5, 29.1.

**Dimeric gold(I) 2,2,5,5-tetramethyl-1,2,3,3a,4,5-hexahydropyrrolo[2,3-b]pyrrolide, 3.** (100 mg, 0.601 mmol) of **1** was suspended in 100 mL of anhydrous THF. Potassium bis(trimethylsilyl)amide (126 mg, 0.633 mmol) was added, at which point all solids quickly dissolved. After stirring for 1 hour, chloro(dimethylsulfide)gold(I) (195 mg, 0.662 mmol) was added as a solid and the reaction mixture was allowed to stir overnight. The reaction mixture was filtered through a Celite pad, and the solvent removed under reduced pressure to afford a white solid that was rapidly washed with 10 mL of cold 1:1 THF:pentane to afford a mixture of diastereomers of **3** (110 mg, 51 %) as a slightly off-white solid. Recrystallization by vapor diffusion of hexanes into a dichloromethane solution of **3** provided white crystals suitable for single-crystal X-ray diffraction. The recrystallized material may be further purified by vacuum sublimation if so desired (180 °C, 30 mTorr). **Elemental Analysis** calcd. for C<sub>20</sub>H<sub>34</sub>Au<sub>2</sub>N<sub>4</sub>: C 33.2%, H 4.73 %, N 7.73 %; found C 33.1%, H 4.56 %, N 7.68%; <sup>1</sup>H NMR (500 MHz, C<sub>6</sub>D<sub>6</sub>) δ 3.15-3.08 (m, 2H), 1.56-1.53 (m, 4H), 1.24 (s, 6H), 1.23 (s, 6H), 1.23-1.19 (m, 4H),1.04 (s, 6H), 1.02 (s, 6H). Mixture of two diastereomers of ratio ca. 43:57, based on integration of the methyl peak areas.

**Tetrameric silver(I) 2,2,5,5-tetramethyl-1,2,3,3a,4,5-hexahydropyrrolo[2,3-b]pyrrolide, 4.** (100 mg, 0.601 mmol) of **1** was suspended in 50 mL of anhydrous Et<sub>2</sub>O. Potassium bis(trimethylsilyl)amide (126 mg, 0.633 mmol) was added, at which point all solids quickly dissolved. After stirring for 1 hour, silver(I) acetate (100 mg, 0.662 mmol) was added as a solid and the reaction mixture was allowed to stir overnight. The reaction mixture was filtered through a Celite pad and the solvent removed under reduced pressure to give an off-white solid. This solid was thoroughly stirred with 500 mL of pentane and filtered again through Celite. Evaporation of the pentane from the filtrate yielded crude **4** (65 mg, 40 %) as a slightly off-white solid. Recrystallization by vapor diffusion of hexanes into a dichloromethane solution of **4** afforded white crystals suitable for single-crystal X-ray diffraction. The recrystallized material may be further purified by vacuum sublimation if so desired (170 °C, 30 mTorr). **Elemental Analysis** calcd. for C<sub>40</sub>H<sub>68</sub>Ag<sub>4</sub>N<sub>8</sub>: C 44.0 %, H 6.27 %, N 10.3 %; found C 44.4%, H 6.22%, N 9.95%.

#### Notes on ligand synthesis.

The key step to the ligand synthesis requires that N,O-bis(trimethylsilyl)acetamide (BSA) be introduced to the reaction very slowly, with the reaction progress carefully monitored by NMR to avoid double trimethylsilylation which results in an unreactive intermediate (Scheme S $\alpha$ ).

#### **Scheme Sa.** Mechanisms of cyclization by BSA.

During the synthesis of the copper complex **2** by the literature route, we found an interesting phenomenon. Despite the copper(I) complex being stable in air, the ESI-TOF MS detection of the compound dissolved in benzene/MeCN showed peaks at m/z ratios of 167 and 395, which correspond to the free ligand and mono-demetalated **2**; no parent ion (m/z = 457) was observed (Figure S1). This result showed that these metal complexes can be labile in MS conditions, in positive ion mode and with formic acid in the mobile phase. Although not quantitative, this signal provides a fast and definitive method of determining the success of the synthesis, which proved to be convenient in the silver and gold precursor syntheses. Similar MS fragmentation and oligomerization patterns have been reported previously for silver(I) amidinates.<sup>2</sup>

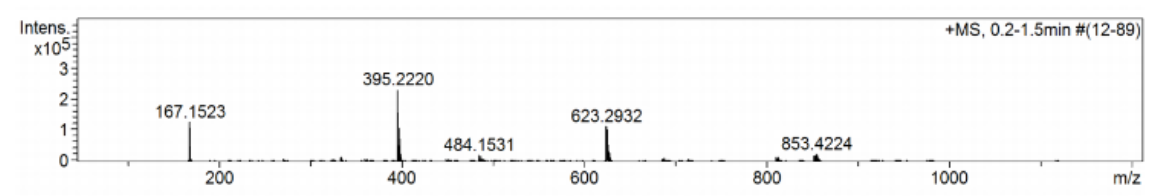


**Figure S1.** Mass-spectrometry data showing the existence of free ligand (m/z = 167), monodemetalated 2 (m/z = 395), and higher clusters of copper ions and ligands generated by the ionization process.

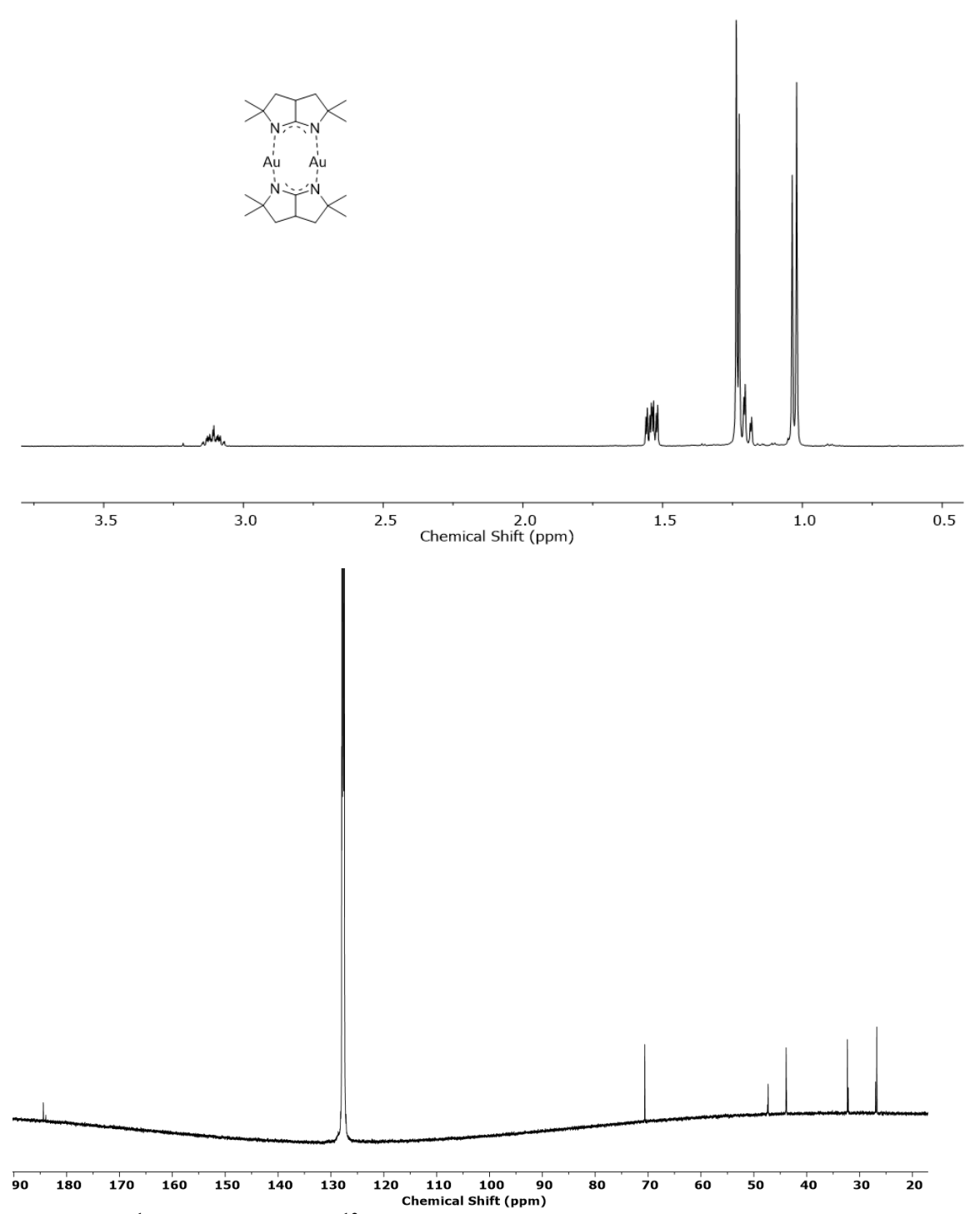


**Figure S2.** <sup>1</sup>H NMR (top) and <sup>13</sup>C NMR (bottom) spectrum of **3**. The doublets indicate the existence of two diastereomers.

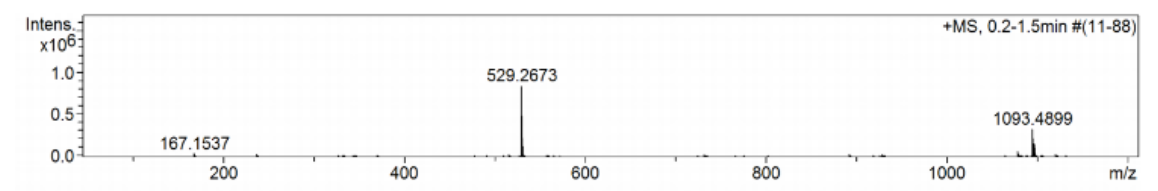


**Figure S3.** Mass-spectrometry data showing the existence of free ligand (m/z = 167), monodemetalated, dimeric 3 (m/z = 529), and a higher cluster of gold ions and ligands generated by the ionization process.

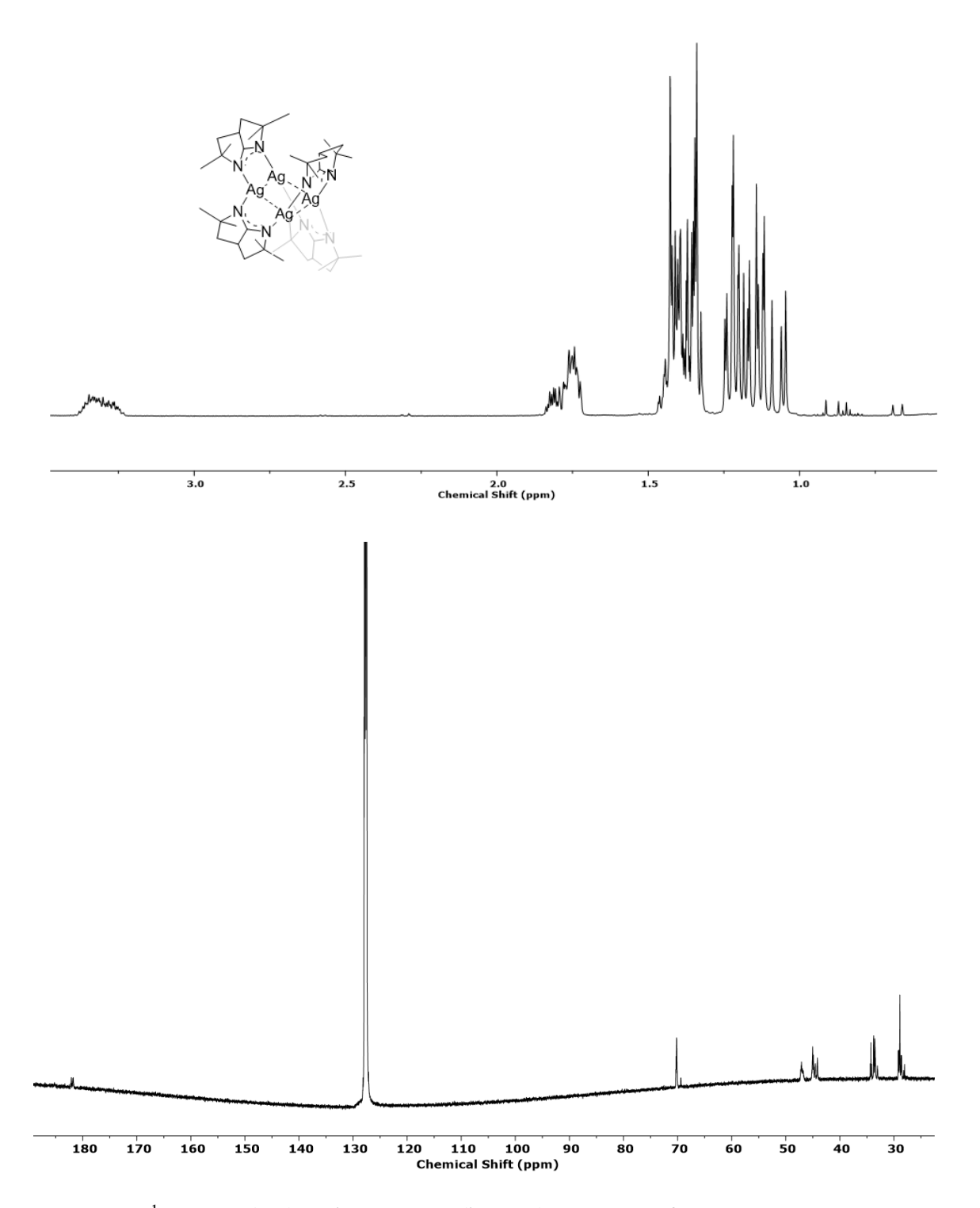


**Figure S4.** <sup>1</sup>H NMR (top) and 13C NMR (bottom) spectrum of **4**.

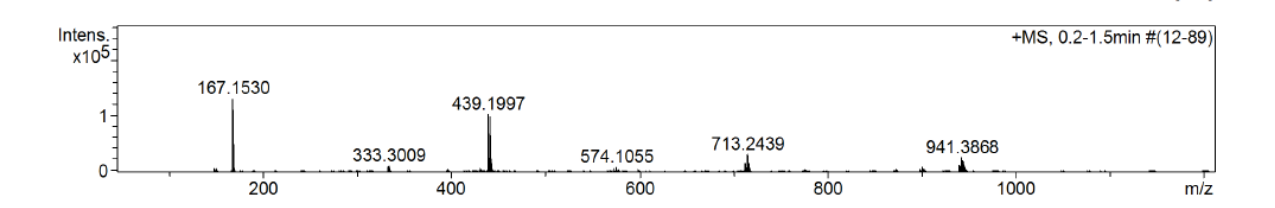


**Figure S5.** Mass-spectrometry data showing the existence of free ligand (m/z = 167), monodemetalated, dimeric 4 (m/z = 439), and higher clusters of silver ions and ligands generated by the ionization process.

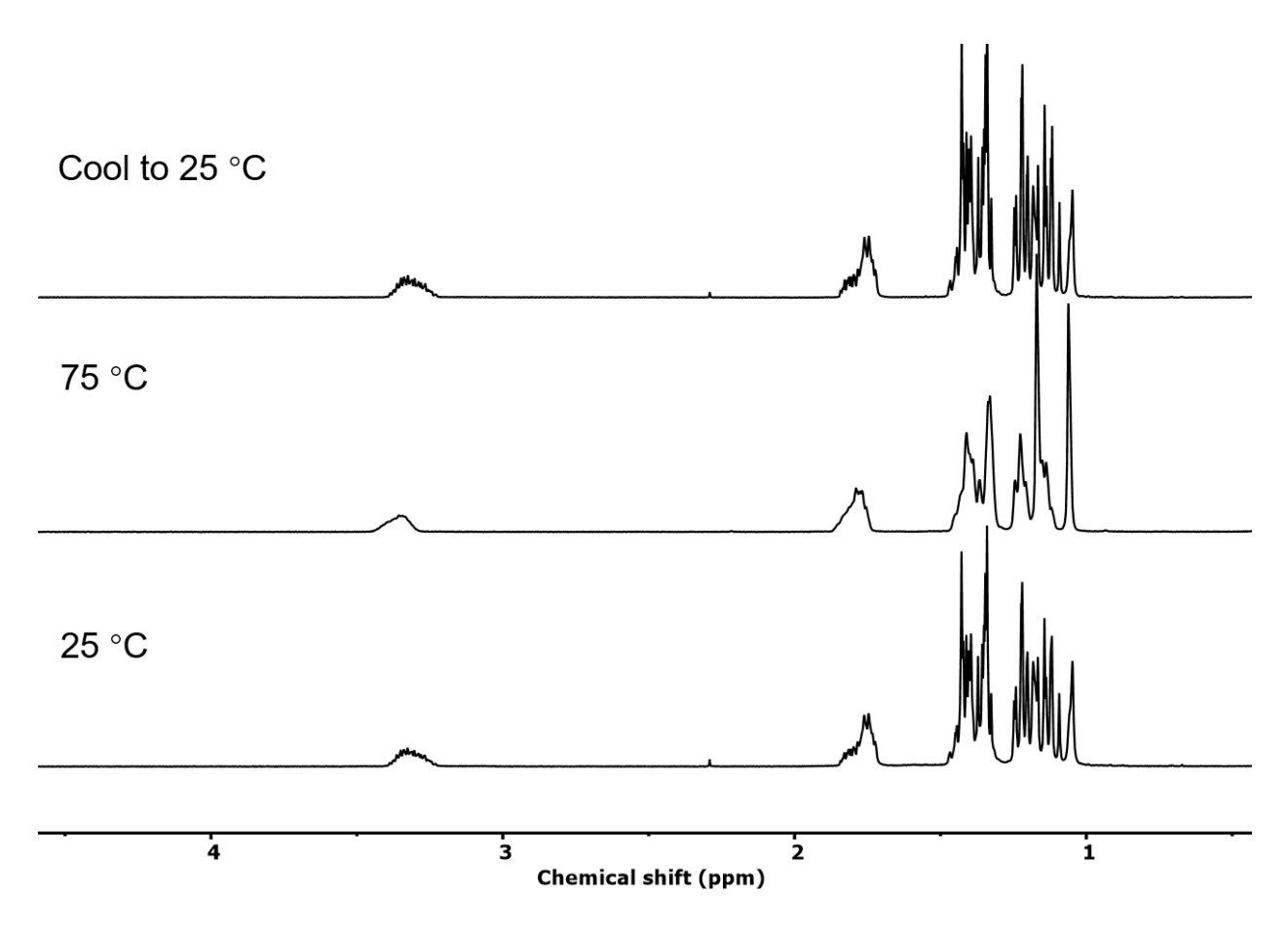


**Figure S6.** Variable-temperature <sup>1</sup>H NMR of **4** in C<sub>6</sub>D<sub>6</sub> showing a reversible simplification of the NMR spectrum, indicating the reversible transition of the tetrameric silver complex to lower order clusters.

Crystallographic Studies.<sup>3</sup> Single crystals of Au<sub>2</sub>(N<sub>2</sub>C<sub>10</sub>H<sub>17</sub>)<sub>2</sub> (3) and Ag<sub>4</sub>(N<sub>2</sub>C<sub>10</sub>H<sub>17</sub>)<sub>4</sub> (4) were grown by vapor diffusion of hexane into dichloromethane at 25 °C. The crystals were mounted on a MiTeGen MicroMount<sup>TM</sup> with Paratone-N oil, and immediately cooled to -173 °C in a cold nitrogen gas stream on the diffractometer, a Bruker three-circle platform goniometer equipped with an Apex II CCD and an Oxford cryostream cooling device. Standard peak search and indexing procedures, followed by least squares refinement, yielded the cell dimensions given in Table S1. Data were collected with an area detector by using the measurement parameters listed in Table S1. The measured intensities were reduced to structure factor amplitudes and their esd's by correction for background, scan speed, Lorentz and polarization effects. No corrections for crystal decay were necessary. Face-indexed absorption corrections were applied, with the absorption coefficient and maximum and minimum transmission factors listed in Table S1. Systematically absent reflections were deleted, and symmetry equivalent reflections were averaged to yield the set of unique data. The remaining 2572 unique data for 3 and 2070 unique data for 4 were used in the least-squares refinements. In the final cycle of least squares refinement, independent anisotropic displacement parameters were refined for the non-hydrogen atoms. All hydrogen atoms were fixed in "idealized" positions with C-H = 0.98 Å (methyl), 0.99 Å (methylene), or 1.00 Å (methine). Methyl groups were allowed to rotate about the C-C axis to find the best least-squares hydrogen atom positions. Isotropic displacement parameters for methyl hydrogen atoms were set to 1.5 times Ueq of the attached carbon, and for methylene and methine groups to 1.2 times Ueq. Successful convergence was indicated by the maximum shift/error of 0.001 for the last cycle. A final analysis of variance between observed and calculated structure factors showed no apparent errors.

4: The orthorhombic lattice and systematic absences for hkl  $(h + k \text{ or } k + l \text{ or } l + h \neq 2n)$ , 0kl  $(k + l \neq 4n)$ , h0l  $(h + l \neq 4n)$ , and hk0  $(h + k \neq 4n)$  were consistent only with space group Fddd, the selection of which was supported by the success of the subsequent refinement. The structure was solved by direct methods (SHELXTL); the correct positions for the silver and nitrogen atoms were deduced from the initial E-map. Subsequent least-squares refinement and difference Fourier calculations revealed the locations of the carbon atoms, including the disordered ones. The quantity minimized in the least-squares program was  $\Sigma w(F_0^2 - F_c^2)^2$ , where  $w = \{[\sigma(F_0^2)]^2 + (0.0140 P)^2\}^{-1}$  and  $P = (F_0^2 + 2F_c^2)/3$ . The carbon atoms not attached to nitrogen atoms were best modeled as disordered over two positions, and the site occupancy factors (SOFs) for the alternative locations were restrained to sum to unity. The SOF of the major component refined to 0.752. No extinction parameter was necessary. The largest peak and hole in the final Fourier difference map (0.40 and -0.27 eÅ<sup>-3</sup>) were located, respectively, 1.13 Å from H3A and 0.57 Å from H7B1.

Table S1. Crystallographic data for compounds  ${\bf 3}$  and  ${\bf 4}$ .

	3	4
formula	Au <sub>2</sub> N <sub>4</sub> C <sub>20</sub> H <sub>34</sub>	Ag4N8C40H68
formula weight	724.45	1092.49
T(K)	100(2)	100(2)
$\lambda$ (Å)	0.71073	0.71073
crystal system	orthorhombic	orthorhombic
space group	Pbca	Fddd
a (Å)	11.691(1)	11.305(2)
b (Å)	10.832(1)	23.157(3)
c (Å)	17.634(1)	33.145(5)
$V(\text{Å}^3)$	2233(1)	8677(2)
$Z$ , $\rho_{\text{calc}}$ (g cm <sup>-3</sup> )	4, 2.155	8, 1.673
$\mu \left(mm^{-1}\right)$	13.134	1.816
F(000)	1360	4416
crystal size (mm)	$0.17 \times 0.17 \times 0.09$	$0.12 \times 0.10 \times 0.05$
θ range (°)	2.31 - 27.54	2.10 - 25.68
R(int)	0.0712	0.0644
absorption correction	face-indexed	face-indexed
max., min. transmission factors	0.878, 0.756	0.922, 0.862
data / restraints / parameters	2572 / 0 / 123	2070 / 229 / 191
GOF on $F^2$	1.069	0.921
$R_1 [I > 2\sigma(I)]$	0.0240	0.0201
$wR_2$ (all data)	0.0669	0.0360
max., min. $\Delta \rho_{elect}$ (e A <sup>-3</sup> )	2.78, -1.31	0.40, -0.27

Table S2. Selected distances (Å) and angles (°) for compound 3.

Au(1)-Au(1A)	2.855(1)	C(3)-C(4)	1.554(5)	N(1A)-C(1)-N(2)	132.5(4)
Au(1)-N(1)	2.013(3)	C(10)-C(7)	1.547(6)	N(1A)-C(1)-C(2A)	113.6(3)
Au(1)-N(2)	2.013(3)	C(4)-C(5)	1.534(6)	N(2)-C(1)-C(2A)	113.9(3)
N(1)-C(1A)	1.324(5)	C(4)-C(6)	1.510(6)	C(1A)-N(1)-C(4)	108.9(3)
N(1)-C(4)	1.492(5)	C(7)-C(8)	1.503(6)	C(1A)-N(1)-Au(1)	119.4(3)
N(2)-C(1)	1.314(5)	C(7)-C(9)	1.536(6)	C(4)-N(1)-Au(1)	131.7(3)
N(2)-C(7)	1.499(4)			C(1)-N(2)-C(7)	109.0(3)
C(1)-C(2)	1.510(5)	N(1)-Au(1)-N(2)	167.4(1)	C(1)-N(2)-Au(1)	120.4(3)
C(2)-C(3)	1.495(6)	N(1)-Au(1)-Au(1A)	83.4(1)	C(7)-N(2)-Au(1)	130.6(3)
C(2)- $C(10)$	1.487(6)	N(2)-Au(1)-Au(1A)	84.0(1)		

**Table S3.** Selected distances (Å) and angles ( $^{\circ}$ ) for compound 4.

3.096(1)	C(1)-C(4)	1.520(4)	C(1)-C(4B)	1.514(8)
3.296(1)	C(2)-C(7)	1.510(4)	C(2)-C(7B)	1.533(8)
3.296(1)	C(2)-C(8)	1.529(4)	C(2)-C(8B)	1.522(7)
3.296(1)	C(2)-C(3)	1.561(4)	C(2)-C(3B)	1.541(7)
5.820(2)	C(3)-C(4)	1.522(5)	C(3B)-C(4B)	1.508(8)
2.094(2)	C(4)-C(5)	1.520(5)	C(4B)-C(5B)	1.507(8)
2.054(2)	C(5)-C(6)	1.555(4)	C(5B)-C(6)	1.555(7)
1.319(3)	C(6)-C(9)	1.525(4)	C(6)-C(9B)	1.518(8)
1.305(3)	C(6)-C(10)	1.522(4)	C(6)-C(10B)	1.514(7)
1.505(3)				
1.496(3)			N(1)-Ag(1)-N(1A)	165.5(1)
	N(1)-C(1)-N(2)	131.9(2)	N(2)-Ag(2)-N(2A)	178.0(1)
129.4(2)	C(1)-N(2)-Ag(2)	123.5(2)	Ag(1)-Ag(2)-Ag(1A)	56.02(1)
122.2(2)	C(6)-N(2)-Ag(2)	127.6(2)	Ag(2)-Ag(1)-Ag(1A)	61.99(1)
107.9(2)	C(1)-N(2)-C(6)	108.8(2)	Ag(2)-Ag(1)-Ag(2A)	124.0(2)
	3.296(1) 3.296(1) 3.296(1) 5.820(2) 2.094(2) 2.054(2) 1.319(3) 1.305(3) 1.505(3) 1.496(3) 129.4(2) 122.2(2)	3.296(1) C(2)-C(7) 3.296(1) C(2)-C(8) 3.296(1) C(2)-C(3) 5.820(2) C(3)-C(4) 2.094(2) C(4)-C(5) 2.054(2) C(5)-C(6) 1.319(3) C(6)-C(9) 1.305(3) C(6)-C(10) 1.505(3) 1.496(3)  N(1)-C(1)-N(2) 129.4(2) C(1)-N(2)-Ag(2) 122.2(2) C(6)-N(2)-Ag(2)	3.296(1) C(2)-C(7) 1.510(4) 3.296(1) C(2)-C(8) 1.529(4) 3.296(1) C(2)-C(3) 1.561(4) 5.820(2) C(3)-C(4) 1.522(5) 2.094(2) C(4)-C(5) 1.520(5) 2.054(2) C(5)-C(6) 1.555(4) 1.319(3) C(6)-C(9) 1.525(4) 1.305(3) C(6)-C(10) 1.522(4) 1.505(3) 1.496(3) N(1)-C(1)-N(2) 131.9(2) 129.4(2) C(1)-N(2)-Ag(2) 123.5(2) 122.2(2) C(6)-N(2)-Ag(2) 127.6(2)	3.296(1) C(2)-C(7) 1.510(4) C(2)-C(7B) 3.296(1) C(2)-C(8) 1.529(4) C(2)-C(8B) 3.296(1) C(2)-C(3) 1.561(4) C(2)-C(3B) 5.820(2) C(3)-C(4) 1.522(5) C(3B)-C(4B) 2.094(2) C(4)-C(5) 1.520(5) C(4B)-C(5B) 2.054(2) C(5)-C(6) 1.555(4) C(5B)-C(6) 1.319(3) C(6)-C(9) 1.525(4) C(6)-C(9B) 1.305(3) C(6)-C(10) 1.522(4) C(6)-C(10B) 1.505(3) 1.496(3) N(1)-Ag(1)-N(1A) N(1)-C(1)-N(2) 131.9(2) N(2)-Ag(2)-N(2A) 129.4(2) C(1)-N(2)-Ag(2) 123.5(2) Ag(1)-Ag(2)-Ag(1A) 122.2(2) C(6)-N(2)-Ag(2) 127.6(2) Ag(2)-Ag(1)-Ag(1A)

**Table S4.** Complete list of angles (°) for compound **3**.

Aton	ı Atom	1 Atom	Angle	Aton	ı Atom	Atom	Angle
N2	Au1	N1	167.44(13)	N1	C4	C3	103.1(3)
N2	Au1	$Au1^1$	83.40(9)	C6	C4	C3	112.9(4)
N1	Au1	Au1 <sup>1</sup>	84.04(10)	C5	C4	C3	111.5(4)
$C1^1$	N1	C4	108.9(3)	N2	C7	C8	109.6(3)
$C1^1$	N1	Au1	119.4(3)	N2	C7	C9	110.0(3)
C4	N1	Au1	131.7(3)	C8	C7	C9	109.9(4)
C1	N2	C7	109.0(3)	N2	C7	$C10^1$	102.7(3)
C1	N2	Au1	120.4(3)	C8	C7	$C10^1$	112.7(4)
C7	N2	Au1	130.6(3)	C9	C7	$C10^1$	111.7(4)
N2	C1	$N1^1$	132.5(4)	C2	C3	C4	105.1(3)
N2	C1	$C2^1$	113.6(3)	C10	C2	C3	130.9(4)
$N1^1$	C1	$C2^1$	113.9(3)	C10	C2	$C1^1$	100.6(3)
N1	C4	C6	109.9(3)	C3	C2	$C1^1$	100.7(3)
N1	C4	C5	109.0(3)	C2	C10	$C7^1$	105.1(4)
C6	C4	C5	110.3(4)				

**Table S5.** Complete angles (°) for compound **4**.

<sup>&</sup>lt;sup>1</sup>: 9/4-X,+Y,1/4-Z; <sup>2</sup>: 9/4-X,5/4-Y,+Z

Atom	Atom	Atom	Angle	Atom	Atom	Atom	Angle
$N1^1$	Ag1	N1	165.47(12)	C8B	C2	C3B	115.8(6)
$N1^1$	Ag1	$Ag1^2$	97.26(6)	C8	C2	C3B	86.3(5)
N1	Ag1	$Ag1^2$	97.26(6)	C7B	C2	C3B	108.8(8)
$N1^1$	Ag1	Ag2	112.71(6)	N1	C2	C3	102.5(2)
N1	Ag1	Ag2	74.50(6)	C7	C2	C3	112.7(3)
$Ag1^2$	Ag1	Ag2	61.988(7)	C8B	C2	C3	138.0(5)
$N1^1$	Ag1	$Ag2^1$	74.50(6)	C8	C2	C3	111.5(3)
N1	Ag1	$Ag2^1$	112.71(6)	C7B	C2	C3	86.4(6)
$Ag1^2$	Ag1	$Ag2^1$	61.986(7)	C3B	C2	C3	26.3(5)
Ag2	Ag1	$Ag2^1$	123.974(13)	C4	C3	C2	103.8(3)
$N2^2$	Ag2	N2	177.98(12)	C1	C4	C5	99.8(3)
$N2^2$	Ag2	$Ag1^2$	80.37(6)	C1	C4	C3	98.5(3)
N2	Ag2	$Ag1^2$	101.44(6)	C5	C4	C3	125.6(5)

N2 <sup>2</sup>	Ag2	Agl	101.44(6)	C5B	C4B	СЗВ	128.3(13)
N2	Ag2	Ag1	80.37(6)	C5B	C4B	C1	96.2(8)
$Ag1^2$	Ag2	Ag1	56.024(13)	C3B	C4B	C1	101.0(8)
C1	N1	C2	107.9(2)	C4	C5	C6	102.0(3)
C1	N1	Ag1	129.37(17)	N2	C6	C10B	111.0(9)
C2	N1	Ag1	122.23(16)	N2	C6	C9B	105.3(7)
C1	N2	C6	108.8(2)	C10B	C6	C9B	113.3(10)
C1	N2	Ag2	123.51(17)	N2	C6	C10	108.7(3)
C6	N2	Ag2	127.57(17)	C10B	C6	C10	25.0(6)
N2	C1	N1	131.9(2)	C9B	C6	C10	91.0(8)
N2	C1	C4B	114.6(5)	N2	C6	C9	113.3(3)
N1	C1	C4B	111.4(4)	C10B	C6	C9	124.8(8)
N2	C1	C4	113.1(3)	C9B	C6	C9	23.3(6)
N1	C1	C4	114.9(3)	C10	C6	C9	107.7(4)
C4B	C1	C4	17.6(7)	N2	C6	C5B	100.9(5)
N1	C2	C7	110.0(3)	C10B	C6	C5B	113.5(7)
N1	C2	C8B	108.8(5)	C9B	C6	C5B	111.9(8)
C7	C2	C8B	82.2(6)	C10	C6	C5B	136.1(6)
N1	C2	C8	109.1(3)	C9	C6	C5B	88.7(5)
C7	C2	C8	110.7(3)	N2	C6	C5	103.5(2)
C8B	C2	C8	31.5(5)	C10B	C6	C5	87.2(6)
N1	C2	C7B	112.9(7)	C9B	C6	C5	134.9(7)
C7	C2	C7B	26.9(6)	C10	C6	C5	111.6(3)
C8B	C2	C7B	105.7(8)	C9	C6	C5	112.1(3)
C8	C2	C7B	129.0(7)	C5B	C6	C5	27.8(4)
N1	C2	C3B	105.0(5)	C4B	C3B	C2	101.5(7)
C7	C2	C3B	132.4(6)	C4B	C5B	C6	105.2(7)

**Table S6.** Distances and angles of the interactions between the gold(I) centers of one molecule of **3** and the methyl groups of its neighbor.

Au···H-C Interaction	d(Au···H), Å	d(Au···C), Å	₄(Au-H-C),°
Au(1E)···H-C(10B)	2.932(2)	3.910(6)	169.6(2)
$Au(1F)\cdots H-C(9A)$	2.968(2)	3.895(6)	158.4(3)
$Au(1F)\cdots H-C(9A)$	3.202(2)	4.072(5)	149.0(3)

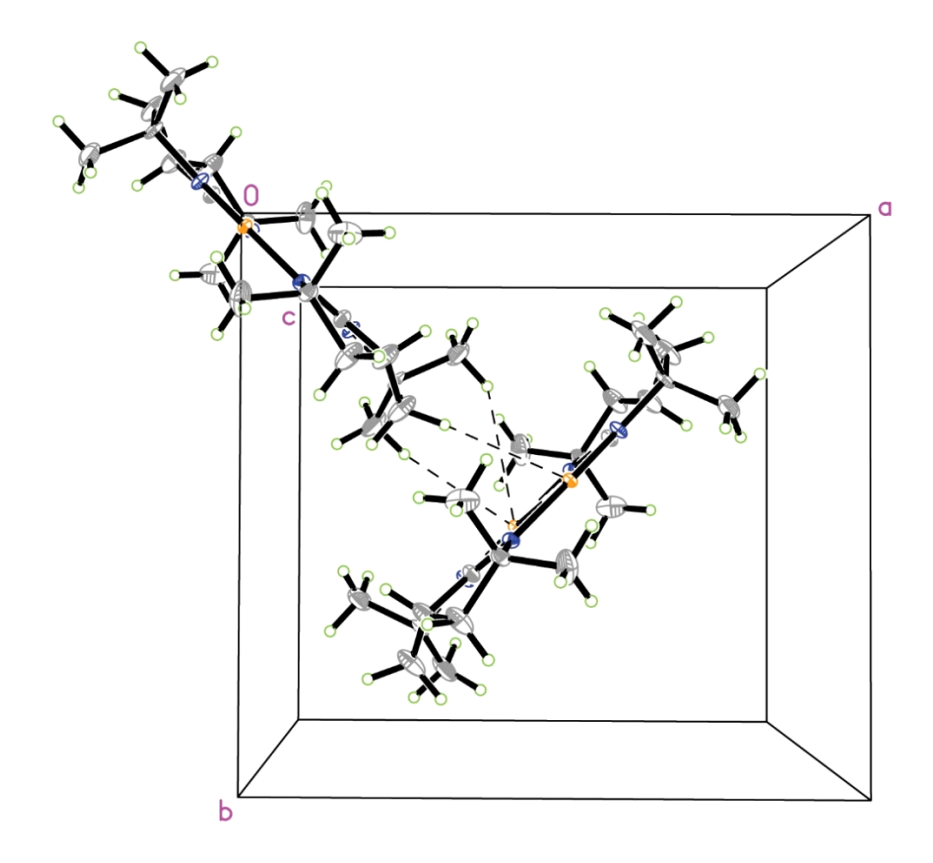


**Figure S7.** Partial packing diagram of **3**, showing the relation between nearest neighbors. Truncated versions of these molecules are shown from a different angle in the main text.

## Comparison of structures to literature compounds.

In **3**, the Au-N distances of 2.013(3) Å are on the shorter end of typical; the reported range is 2.025(9)-2.085(7) Å in digold(I)<sup>4-7</sup> amidinates and 2.000(4)-2.057(11) Å in tetragold(I) complexes.<sup>8-11</sup> The Au····Au distance is 2.855(1) Å, more similar to the 2.902(1)-3.049(1) Å found in tetragold(I) amidinates<sup>8-10</sup> than the 2.644(2)-2.711(3) Å reported for other digold(I) amidinates.<sup>4-7</sup> In **3**, the combination of the short Au-N distances and the N-C-N angle leads to bent N-Au-N angles of 167.4(1)°. Gold(I) amidinate and guanidinate dimers typically have N-Au-N angles of 167.7(3)°-170.8(4)°,<sup>4-7</sup> however, so this effect is not strong.

In **4**, the N-Ag-N angles are asymmetric, with one angle approaching the preferred linear coordination geometry of silver(I), 178.0(1)°, and the other substantially contracted to 165.5(1)°. This asymmetry is not unusual, with N-Ag-N angles varying as much as 156.3(2)° to 178.4(2)° within a single tetranuclear molecule.<sup>2, 12</sup> Although the Ag···Ag distances of 3.296(2) Å along the sides of **4** are unusually long, the cross distance of 3.096(2) Å (Ag(1)···Ag(1A)) falls into the previously observed range of 3.077(1)-3.220(1) Å.<sup>2, 12</sup> Disilver(I) and trisilver(I) complexes typically have shorter Ag···Ag distances also, in the range of 2.645(1)-2.754(1) Å<sup>4, 13-15</sup> and 2.955(1)-3.217(1) Å,<sup>6, 7, 13</sup> respectively.

Regarding the disorder in **4**, the high symmetry of the site on which the molecule sits in the unit cell prevents us from determining the distribution of this conformation across molecules in the lattice (e.g., whether, say, ½ of the molecules have every ligand inverted, or every molecule has ¼ of the ligands inverted).

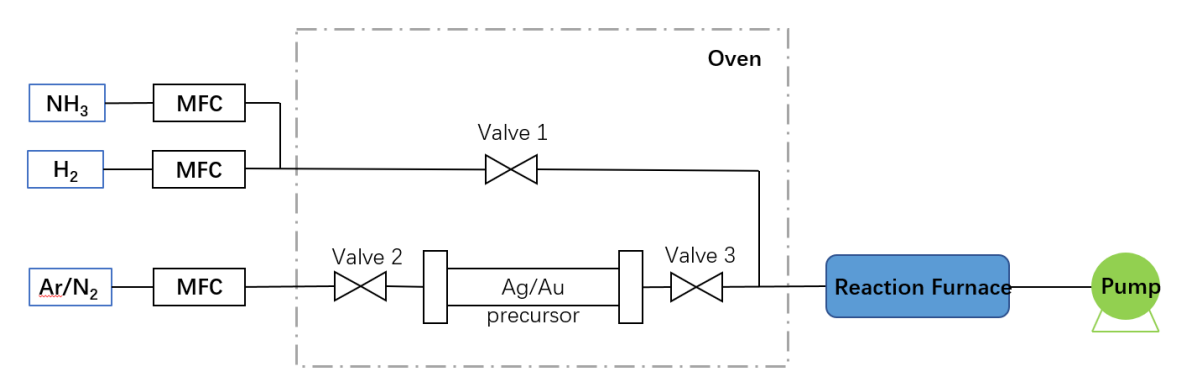
**Thermogravimetric Analysis (TGA).** TGA experiments were performed with a TA Instruments Model Q50 system in a glovebox.  $N_2$  was used as the flow gas (balance gas: 40 mL/min, sample gas: 40.0 mL/min). Aluminum sample pans (100  $\mu$ L, TA Instruments Cat. #: 952323.902) with diameter 1 cm were used for this experiment; a new pan was used for each experiment.

**Ramp TGA experiments:** ca. 10 mg of **2**, **3**, and **4** were used for ramp TGA with a heating rate of 10 °C/min.

**Isothermal TGA experiments:** These experiments were performed to obtain the temperature dependence of the evaporation rate. In a typical experiment, a sample pan was loaded with ca. 10 mg of sample material, and then heated at 10 °C/min to the first isotherm temperature. After the temperature stabilized, it was maintained for 11 minutes to collect isothermal weight loss data at that temperature. The temperature was then raised to the next isotherm temperature following the same protocol. The isotherm temperatures were 170, 180, 190, 200, 210, 220, 230 °C. A plot of ln(rate constant of sublimation) vs the reciprocal of temperature in Kelvin yields the slope as the activation energy for sublimation according to the Arrhenius equation:

$$\ln(k) = \ln(A) - \frac{E_a}{RT}$$

## CVD of gold and silver thin films



**Scheme 1.** Schematics of home-made CVD reactor

The CVD of gold and silver is conducted in a flow-through-type CVD reactor described in detail previously, <sup>16</sup> the precursor delivery system of which is illustrated in Scheme 2. In detail, the molecular precursor **3** or **4** is stored in a tube-shape glass container with CF flange connectors at both ends. After being heated to ca. 160-180 °C, the precursor is delivered into the reaction chamber with a flow (100 sccm) of Ar or N<sub>2</sub> carrier gas. At the same time, continuous flow of purified H<sub>2</sub> gas is delivered into the reaction chamber to mix with the precursor, reducing the precursor to metal films. The reaction chamber is heated by a tube furnace and a built-in substrate heater. The substrate is heated to a slightly higher temperature (~10 °C) than the surrounding tube wall, so that the deposition mainly occurs on the substrates. We used thermal oxide silicon (300 nm of wet-oxidation SiO<sub>2</sub> on Si) coupons and glass slides as the substrates for depositions.

# Characterization of gold and silver films

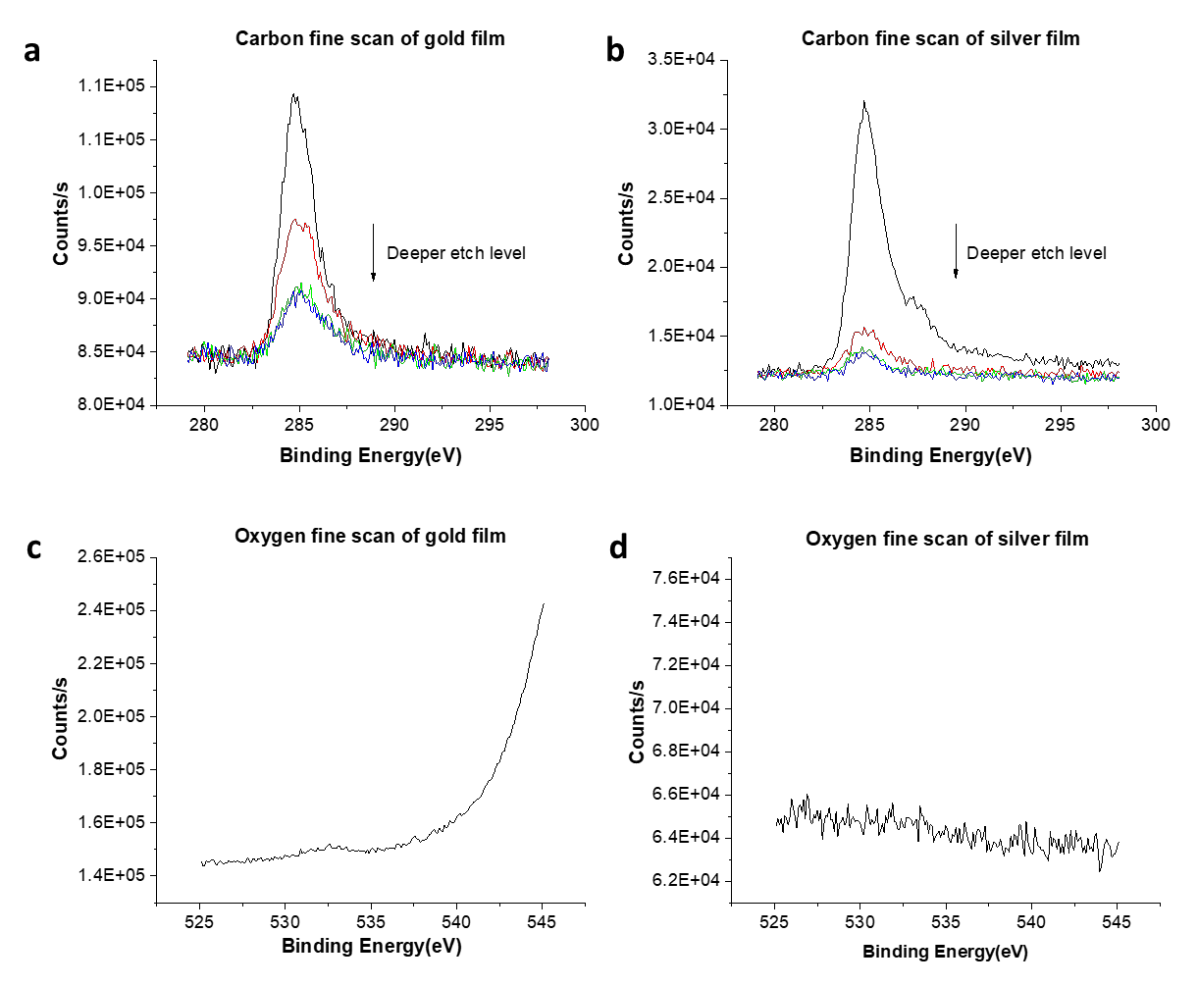


**Figure S8.** a) Carbon fine scans of a CVD gold film at several etch levels. b) Carbon fine scan of a CVD silver film at several etch levels. c) Oxygen fine scan of a CVD gold film at the deepest etch level. d) Oxygen fine scan of a CVD silver film at the deepest etch level.

XPS carbon fine scans demonstrate that carbon peaks of both gold and silver film decrease as etching levels go deeper. Atomic percentage of carbon was calculated based on the area of all peaks and XPS relative sensitivity factors.

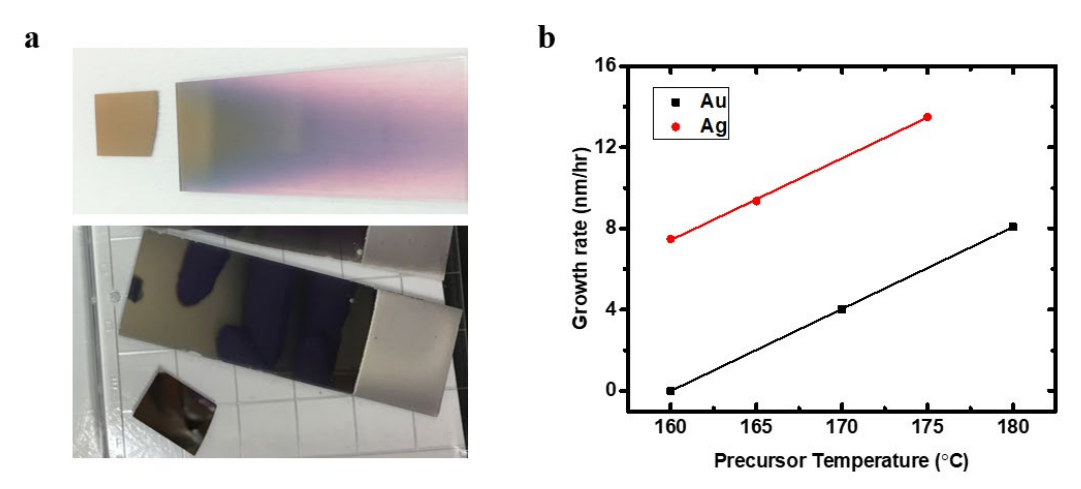


**Figure S9. a)** Photos of deposited gold film (top) and silver film (bottom). **b)** growth rate increases linearly with precursor temperature.

**Table S7.** Selected gold depositions with conditions and their corresponding growth and electrical properties.

	Selected Gold Depositions Summary								
No.		Depo	sition Condition	Thickness (nm) /	Conductivity				
	Bub T (°C)	Sub T (°C)	Gas	Time (hrs)	Growth Rate (nm/hrs)	(Ω.nm)			
Au 005	170	230/235	100 N <sub>2</sub>	13	No film	Not conductive			
Au 006	170	230/235	100:100 H <sub>2</sub> :N <sub>2</sub>	6.5	100.1 / 15.4	245.31			
Au 008	185	200/208	100:100 H <sub>2</sub> :N <sub>2</sub>	14	123.3 / 8.8	221.94			
Au 009	185	200/209	100:100:100 H <sub>2</sub> :N <sub>2</sub> :NH <sub>3</sub>	15	53.35/3.56	250.75			

**Table S8.** Selected silver depositions with conditions and their corresponding growth, elemental composition, and electrical properties.

			Selected	Silver	Depositions Sum	mary			
No.	Deposition Condition			Thickness	XPS Composition			Conductivity	
Bub T	Bub T	T Sub T (°C)	T (°C) Gas	Time	(nm) / Growth	(Deep	(Deepest etching		(Ω.nm)
	(°C)	(hrs)	(hrs)	Rate (nm/hrs)	Ag	С	0		
Ag 002	160	200/209	100:100 H <sub>2</sub> :N <sub>2</sub>	14	66 / 5.08	61.04	35.14	3.82	2224
Ag 010	170	229/232	100:100 H <sub>2</sub> :Ar	18	168.33 / 9.35	83.5	16.5	0	1500
Ag 011	170	225/232	200:100 H <sub>2</sub> :Ar	18	238.2 / 14.01	93.39	6.61	0	192.5
Ag 012	170	217/231	100 Ar	17	20 / 1.18	23.37	47.91	14.33	Not

#### References

- 1. E. S. Beh, L. Tong and R. G. Gordon, *Organometallics*, 2017, **36**, 1453-1456.
- 2. S. J. Archibald, N. W. Alcock, D. H. Busch and D. R. Whitcomb, *J. Cluster Sci.*, 2000, 11, 261-283.
- 3. J. L. Brumaghim, J. G. Priepot and G. S. Girolami, *Organometallics*, 1999, **18**, 2139-2144.
- 4. D. Fenske, G. Baum, A. Zinn and K. Dehnicke, Z. Naturforsch. B, 1990, 45, 1273-1278.
- 5. H. E. Abdou, A. A. Mohamed and J. John P. Fackler, *Inorg. Chem.*, 2005, 44, 166-168.
- 6. T. J. J. Whitehorne, J. P. Coyle, A. Mahmood, W. H. Monillas, G. P. A. Yap and S. T. Barry, *Eur. J. Inorg. Chem.*, 2011, 3240-3247.
- 7. S. K. Adas, J. A. Ocana and S. D. Bunge, *Aust. J. Chem.*, 2014, **67**, 1021-1029.
- 8. E. Hartmann and J. Strähle, Z. Naturforsch. B, 1989, 44, 1-4.
- 9. A. A. Mohamed, H. E. Abdou, M. D. Irwin, J. M. López-de-Luzuriaga and J. John P. Fackler, *J. Cluster Sci.*, 2003, **14**, 253-266.
- 10. H. E. Abdou, A. A. Mohamed, J. M. López-de-Luzuriaga and J. John P. Fackler, *J. Cluster Sci.*, 2004, **15**, 397-411.
- 11. A. A. Mohamed, A. P. Mayer, H. E. Abdou, M. D. Irwin, L. M. Pérez and J. John P. Fackler, *Inorg. Chem.*, 2007, **46**, 11165-11172.
- 12. M. D. Irwin, H. E. Abdou, A. A. Mohamed and J. John P. Fackler, *Chem. Commun.*, 2003, 2882-2883.
- 13. B. S. Lim, A. Rahtu, J.-S. Park and R. G. Gordon, *Inorg. Chem.*, 2003, **42**, 7951-7958.
- 14. A. C. Lane, M. V. Vollmer, C. H. Laber, D. Y. Melgarejo, G. M. Chiarella, J. John P. Fackler, X. Yang, G. A. Baker and J. R. Walensky, *Inorg. Chem.*, 2014, **53**, 11357-11366.
- 15. S. Wang, N. Harmgarth, P. Leibing and F. T. Edelmann, *Acta Cryst.*, 2016, **E72**, 1786-1790.
- 16. Y. Au, Y. Lin and R. G. Gordon, *J. Electrochem. Soc.*, 2011, **158**, D248-D253.